IOP PUBLISHING NONLINEARITY

Nonlinearity **24** (2011) 1271–1289 doi:10.1088/0951-7715/24/4/013

Variational approximations of trapped vortices in the large-density limit

D E Pelinovsky[1] **and P G Kevrekidis**[2]

[1] Department of Mathematics and Statistics, McMaster University, Hamilton, Ontario, L8S 4K1, Canada
[2] Department of Mathematics and Statistics, University of Massachusetts, Amherst, MA 01003, USA

Received 4 August 2010, in final form 17 January 2011
Published 11 March 2011
Online at stacks.iop.org/Non/24/1271

Recommended by M J Peyrard

Abstract
The Gross–Pitaevskii equation with a harmonic potential and repulsive nonlinear interactions is considered in the large-density limit, also known as the Thomas–Fermi limit. In two space dimensions, we employ the Rayleigh–Ritz method to obtain variational approximations of single vortices, dipole pairs and quadrupoles trapped in the harmonic potential. In particular, we compute the eigenfrequency of the single vortex precession about the centre of symmetry of the harmonic potential, as well as the eigenfrequencies of the oscillations of the dipole and quadrupole vortex configurations. The asymptotic results are compared to numerical computations.

Mathematics Subject Classification: 35Q55, 37K45, 37K50

(Some figures in this article are in colour only in the electronic version)

1. Introduction

In the realm of Bose–Einstein condensates (BECs) with self-repulsive interatomic interactions, vortices constitute the prototypical higher-dimensional nonlinear excitations [27, 29]. Such nonlinear waves have been examined in a wide range of studies, not only from a theoretical standpoint but also from an experimental one, as has now been summarized in numerous specialized reviews of this research theme [3, 8, 9]. Recently, there has been a renewed interest in the topic due to the emerging ability to create a few such vortices, such as two [23] and three [31], and even to observe their ensuing dynamics in a minimally destructive manner [10].

In the case of a parabolic confinement, which is typical in BECs, single vortices are well known to precess about the centre of symmetry of the harmonic potential. The combination of such precession with the inter-vortex interactions is the driving force for the complex vortex dynamics that ensue in the BEC setting. It is these precessional and interacting vortex dynamics

that we will focus on in this work. In particular, we will consider the large-density limit, in the context of the prototypical mean-field model for the BECs, namely the Gross–Pitaevskii equation. Our analysis will be carried out by means of the Rayleigh–Ritz method.

Several variational approximations of trapped vortices in the space of two dimensions were reported in the recent past. Möttönen *et al* [22] computed the interaction energy for dipole, tripole and quadrupole configurations (i.e. for two, three and four vortices, respectively) and showed that the interaction energy has an effective maximum where a stationary configuration is possible. The variational ansatz was not discussed in [22]. Li *et al* [19] gave more details on the variational ansatz and the underlying dynamics of the vortex–antivortex pair in the harmonic potential using trajectories on a phase plane. The variational ansatz in [19] was a product of linear functions and the ground state of the Gross–Pitaevskii equation. The dipole configuration was found to bifurcate for a finite chemical potential and to persist as a stable solution in the large-density limit.

In addition to variational results, several other approximations are relevant in the context of the Gross–Pitaevskii equation with a harmonic potential (and especially, in connection with the large-density limit). Gallo and Pelinovsky [11] justified the Thomas–Fermi approximation of the ground state in the space of one, two and three dimensions using the Painlevé-II equation. A variational characterization of the ground state and the charge-one vortex in the Thomas–Fermi limit was earlier developed by Ignat and Millot [13, 14]. Kevrekidis and Pelinovsky [15] computed the asymptotic distribution of eigenvalues of the spectral stability problem for the ground state and compared it with earlier results of Stringari [32] and others.

Other approaches based on the numerical simulations have also been developed, starting with earlier works of Crasovan *et al* [6] and Klein *et al* [17] among others. Kollar and Pego [18] constructed numerical approximations of eigenvalues of the spectral stability problem for single vortices and found islands of instability for vortices of topological charge two and higher. Approximations of the lowest eigenvalue for the stable charge-one vortex were discussed by Middelkamp *et al* [20] based on the method of matched asymptotic expansions [16]. The lowest eigenfrequency of the stable vortex gives the frequency of precession of the vortex within the harmonic potential and it is an important quantity in the characterization of the vortex dynamics under some perturbations such as the inhomogeneous interatomic interactions and finite temperatures [20]. Recently, single vortices, dipoles, quadrupoles and other vortex structures were studied numerically by Middelkamp *et al* [21].

The aim of this work is to provide a systematic derivation of the variational approximations for single vortices as well as for the multi-vortex configurations such as dipole pairs and quadrupoles. These are the simplest and most robust (potentially stable) vortex configurations which have been discovered numerically and, in most cases, also analysed experimentally in the physics literature.

Our variational ansatz is a product of a ground state in the Gross–Pitaevskii equation with a harmonic potential and the vortices in the defocusing nonlinear Schrödinger equation. This ansatz relies on the vortex construction in the rigorous existence theory [13, 14] and this is the key difference of our work from the previous variational approximations obtained in [19, 22]. We also obtain an asymptotic formula of the lowest eigenfrequency of oscillations of the charge-one vortex in the large-density limit. Ironically, the optimal constant does not give a better comparison with the numerical data for smaller values of the chemical potential than the numerical fit constructed by Middelkamp *et al* [20, 21]. Nevertheless, as the relevant chemical potential parameter is increased, the asymptotic result approaches the obtained numerical approximation (i.e. the two share the same asymptotic dependence on the chemical potential).

The energy and dynamics of vortex configurations in the defocusing nonlinear Schrödinger equation were previously considered by Ovchinnikov and Sigal [24, 25]. Compared with these

works, the energy of the Gross–Pitaevskii equation with a harmonic potential does not need to be renormalized because the vortices supported on the ground state always have a finite energy. The interaction energy of the vortex–antivortex pair is obtained from the logarithmic Kirchhoff–Onsager Hamiltonian justified in [24, 25]. This logarithmic dependence of the interaction energy is reminiscent of that for inviscid fluid vortices, whereby the velocity field induced by each vortex affects the kinematics of the vortices around it (and vice versa) [4].

From a technical standpoint, this work is a continuation (and generalization in higher dimensions) of our previous studies of dark solitons in the defocusing Gross–Pitaevskii equation with a harmonic potential in one spatial dimension [5, 26]. Unlike the variational approximations of dark solitons in [5], we have to compute the relevant integrals in the implicit form. The rigorous justification of the asymptotic approximations of the vortex configurations as the product of the ground state and the free vortex can be developed similarly to [26] and will not be discussed here.

The paper is organized as follows. Section 2 reviews the properties of the ground states in the large-density limit. Section 3 reports the variational approximations of individual vortices. Dipole and quadrupole configurations are considered in sections 4 and 5 respectively. Section 6 offers some interesting directions for future studies. The appendix gives a summary of the asymptotic representation of the ground states, which is used in the computations of vortex approximations.

2. Mathematical setup

Let us start with the Gross–Pitaevskii equation with a harmonic potential and repulsive nonlinear interactions

$$\mathrm{i}U_\tau = -\tfrac{1}{2}(U_{\xi_1\xi_1} + U_{\xi_2\xi_2}) + \tfrac{1}{2}(\xi_1^2 + \xi_2^2)U + |U|^2U - \mu U, \tag{1}$$

where $U(\xi_1, \xi_2, \tau) : \mathbb{R}\times\mathbb{R}\times\mathbb{R} \to \mathbb{C}$ is the wave function and $\mu \in \mathbb{R}$ represents the chemical potential (the number of atoms in the condensate). We are interested in localized modes of the Gross–Pitaevskii equation in the large-density limit $\mu \to \infty$, which is associated with the Thomas–Fermi limit. Using the scaling transformation,

$$U(\xi_1, \xi_2, \tau) = \mu^{1/2}u(x_1, x_2, t), \qquad \xi_{1,2} = (2\mu)^{1/2}x_{1,2}, \qquad \tau = 2t, \tag{2}$$

the Gross–Pitaevskii equation (1) is transformed to the semi-classical form

$$\mathrm{i}\varepsilon u_t + \varepsilon^2\nabla^2 u + (1 - |x|^2 - |u|^2)u = 0, \tag{3}$$

where $x = (x_1, x_2) \in \mathbb{R}^2$, $|x|^2 = x_1^2 + x_2^2$, $\nabla^2 = \partial_{x_1}^2 + \partial_{x_2}^2$ and $\varepsilon = (2\mu)^{-1}$ is a small parameter.

Let η_ε be a real positive solution of the stationary problem

$$\varepsilon^2\nabla^2\eta_\varepsilon + (1 - |x|^2 - \eta_\varepsilon^2)\eta_\varepsilon = 0, \qquad x \in \mathbb{R}^2. \tag{4}$$

The main results of Ignat and Millot [13, 14] and Gallo and Pelinovsky [11] state that for any sufficiently small $\varepsilon > 0$ there exists a smooth solution $\eta_\varepsilon \in C^\infty(\mathbb{R}^2)$ that decays to zero as $|x| \to \infty$ faster than any exponential function. More precisely, there is $C > 0$ such that

$$0 < \eta_\varepsilon(x) \leqslant C\varepsilon^{1/3}\exp\left(\frac{1 - |x|^2}{4\varepsilon^{2/3}}\right), \qquad \text{for all } |x| \geqslant 1. \tag{5}$$

The ground state converges pointwise as $\varepsilon \to 0$ to the compact Thomas–Fermi cloud

$$\eta_0(x) := \lim_{\varepsilon\to 0}\eta_\varepsilon(x) = \begin{cases}(1 - |x|^2)^{1/2}, & x \in D_0,\\ 0, & x \notin D_0,\end{cases} \tag{6}$$

where D_0 is the unit disc in $\mathbb{R}^2$ centred at the origin. By proposition 2.1 in [13], for any compact subset $K \subset D_0$, there is $C_K > 0$ such that

$$\|\eta_\varepsilon - \eta_0\|_{C^1(K)} \leqslant C_K \varepsilon^2. \tag{7}$$

The error bound (7) cannot be justified uniformly for all $x \in \mathbb{R}^2$ because of the singular behaviour of derivatives of $\eta_\varepsilon(x)$ near the boundary of D_0. The uniform bound was obtained in [11], namely, there is $C > 0$ such that

$$\|\eta_\varepsilon - \eta_0\|_{L^\infty} \leqslant C\varepsilon^{1/3}. \tag{8}$$

Justification of the uniform bound (8) is reviewed in appendix as some details are relevant for this work.

We shall consider stationary vortices of the Gross–Pitaevskii equation (3), which are non-positive non-real solutions of the stationary problem

$$\varepsilon^2 \nabla^2 u_\varepsilon + (1 - |x|^2 - |u_\varepsilon|^2) u_\varepsilon = 0, \qquad x \in \mathbb{R}^2. \tag{9}$$

We shall apply variational approximations to study relative dynamics of vortices with respect to the harmonic potential and to each other. In particular, we obtain results concerning the existence of stationary vortices and the lowest eigenfrequencies of the vortex oscillations from the Euler–Lagrange equations generated by an effective Lagrangian computed at the vortex configurations. To enable this formalism, we substitute

$$u(x,t) = \eta_\varepsilon(x) v(x,t), \qquad x \in \mathbb{R}^2, \qquad t \in \mathbb{R},$$

to the Gross–Pitaevskii equation (3) and find an equivalent equation

$$\mathrm{i}\varepsilon \eta_\varepsilon^2 v_t + \varepsilon^2 \nabla \cdot \left(\eta_\varepsilon^2 \nabla v\right) + \eta_\varepsilon^4 (1 - |v|^2) v = 0. \tag{10}$$

The Gross–Pitaevskii equation (10) follows from the Lagrangian function $L(v) = K(v) + \Lambda(v)$ by means of the Euler–Lagrange equations

$$\frac{\delta L}{\delta \bar{v}} - \frac{\mathrm{d}}{\mathrm{d}t} \frac{\delta L}{\delta \bar{v}_t} = 0,$$

where the kinetic energy is

$$K(v) = \frac{\mathrm{i}}{2} \varepsilon \int_{\mathbb{R}^2} \eta_\varepsilon^2 (v \bar{v}_t - \bar{v} v_t) \, \mathrm{d}x \tag{11}$$

and the (negative) potential energy is

$$\Lambda(v) = \varepsilon^2 \int_{\mathbb{R}^2} \eta_\varepsilon^2 |\nabla v|^2 \, \mathrm{d}x + \frac{1}{2} \int_{\mathbb{R}^2} \eta_\varepsilon^4 (1 - |v|^2)^2 \, \mathrm{d}x. \tag{12}$$

In what follows, we substitute an appropriate variational ansatz representing particular vortex configurations to the integrals (11) and (12). Instead of notations $(x_1, x_2) \in \mathbb{R}^2$, we will use notations $(x, y) \in \mathbb{R}^2$. We denote $R = \mathcal{O}(\varepsilon + x_0^2 + y_0^2)$ if

$$\exists C > 0 : \quad |R| \leqslant C \left(\varepsilon + x_0^2 + y_0^2\right),$$

for small $\varepsilon > 0$ and $(x_0, y_0) \in \mathbb{R}^2$. The constant $C > 0$ can change from one line to another line.

3. Single vortices

We shall consider the variational approximation of a single vortex, which is confined near the centre of the harmonic potential. Using the Euler–Lagrange equations for the effective Lagrangian, we obtain the frequency of precession of the single vortex about the centre of the harmonic potential for small $\varepsilon > 0$ (or large $\mu > 0$). This frequency is subsequently compared with the numerical approximations of eigenvalues of the linearization around the stationary vortex for all values of the chemical potential μ.

3.1. Free vortex

Let (r, θ) represent polar coordinates on the plane $(x, y) \in \mathbb{R}^2$ centred at the point $(x_0, y_0) \in \mathbb{R}^2$, that is

$$x = x_0 + r\cos(\theta), \qquad y = y_0 + r\sin(\theta).$$

If $\eta_\varepsilon \equiv 1$, the Gross–Pitaevskii equation (10) is written as the defocusing NLS equation

$$\mathrm{i}\varepsilon v_t + \varepsilon^2\nabla^2 v + (1 - |v|^2)v = 0. \tag{13}$$

The stationary (t-independent) vortex of the NLS equation (13) has the form

$$v(x, y) = V_m(x - x_0, y - y_0) = \Psi_m(R)\mathrm{e}^{\mathrm{i}m\theta}, \qquad R = \frac{r}{\varepsilon}, \tag{14}$$

where $m \in \mathbb{N}$ is referred to as the vortex charge. The envelope function $\Psi_m(R)$ is a solution of the second-order differential equation

$$\frac{\mathrm{d}^2\Psi_m}{\mathrm{d}R^2} + \frac{1}{R}\frac{\mathrm{d}\Psi_m}{\mathrm{d}R} - \frac{m^2}{R^2}\Psi_m + (1 - \Psi_m^2)\Psi_m = 0, \qquad R > 0, \tag{15}$$

such that $\Psi_m(0) = 0$, $\Psi_m(R) > 0$ for all $R > 0$, and $\lim_{R\to\infty}\Psi_m(R) = 1$.

Existence and uniqueness of solutions of the boundary-value problem for (15) is well known in the literature on vortices [1, 28]. Analysing differential equations with regular singular points, one can easily show that Ψ_m is a $\mathcal{C}^\infty$ function for all $R > 0$ and there is $\alpha_m > 0$ such that

$$\Psi_m(R) = \alpha_m R^m + \mathcal{O}(R^{m+2}) \qquad \text{as} \quad R \to 0 \tag{16}$$

and

$$\Psi_m^2(R) = 1 - \frac{m^2}{R^2} + \mathcal{O}\left(\frac{1}{R^4}\right) \qquad \text{as} \quad R \to \infty. \tag{17}$$

We note that the potential energy (12) for the free vortex (14) diverges logarithmically if $\eta_\varepsilon \equiv 1$. The renormalized energy for the free vortex can be proposed in the form

$$\Lambda_R^{(m)}(\Phi) = \int_0^\infty \left[\left(\frac{\mathrm{d}\Phi}{\mathrm{d}R}\right)^2 + \frac{m^2}{R^2}\left(\Phi^2 - \frac{R^2}{1+R^2}\right) + \frac{1}{2}(1 - \Phi^2)^2\right] R\,\mathrm{d}R, \tag{18}$$

which recovers equation (15) from the Euler–Lagrange equation

$$\left.\frac{\delta\Lambda_R^{(m)}}{\delta\Phi}\right|_{\Phi=\Psi_m} = 0.$$

Note that $\Lambda_R^{(m)}(\Psi_m)$ is scaled by $2\pi\varepsilon^2$ compared with $\Lambda(V_m)$.

Let us consider the dilation transformation

$$\Phi(R) = \Psi_m\left(\frac{R}{a}\right), \qquad a > 0,$$

where $\Psi_m(R)$ is a solution of the second-order equation (15). The energy functional (18) becomes

$$F(a) := \Lambda_R^{(m)}(\Phi) = \int_0^\infty \left[\left(\frac{\mathrm{d}\Psi_m}{\mathrm{d}R}\right)^2 + \frac{m^2}{R^2}\left(\Psi_m^2 - \frac{a^2R^2}{1+a^2R^2}\right) + \frac{a^2}{2}(1 - \Psi_m^2)^2\right] R\,\mathrm{d}R.$$

Since Ψ_m is a critical point of $\Lambda_R(\Phi)$ that corresponds to $a = 1$, we have necessarily $F'(1) = 0$, which gives, through direct differentiation, the constraint

$$\int_0^\infty (1 - \Psi_m^2)^2 R\,\mathrm{d}R = 2m^2\int_0^\infty \frac{R\,\mathrm{d}R}{(1+R^2)^2} = m^2. \tag{19}$$

Constraint (19) was first derived by Brezis *et al* [2].

We can approximate solutions Ψ_m using an elementary shooting method [7]. The numerical approximations for $m = 1$ and $m = 2$ are shown in figure 1.

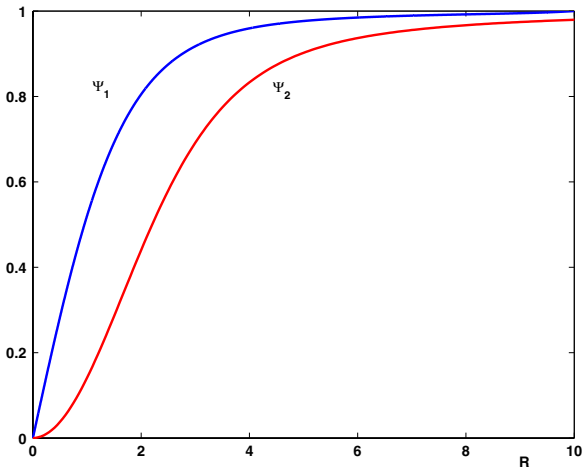

Figure 1. Profiles of Ψ_1 and Ψ_2 obtained by the shooting method.

3.2. Kinetic energy

We can now substitute the variational ansatz (14) into the kinetic energy (11) for the Gross–Pitaevskii equation (10) with $\eta_\varepsilon \not\equiv 1$. Recall that D_0 denotes the unit disc in $\mathbb{R}^2$, where the compact limiting function η_0^2 is non-zero. In variables

$$x = x_0 + \varepsilon X, \qquad y = y_0 + \varepsilon Y,$$

the unit disc D_0 transforms to the disc

$$D_\varepsilon(x_0, y_0) = \left\{ (X, Y) \in \mathbb{R}^2 : \quad \left(X + \frac{x_0}{\varepsilon}\right)^2 + \left(Y + \frac{y_0}{\varepsilon}\right)^2 < \frac{1}{\varepsilon^2} \right\}.$$

We shall prove the following.

Lemma 1. *For small $\varepsilon > 0$ and $(x_0, y_0) \in \mathbb{R}^2$, the kinetic energy of a single vortex is expanded by*

$$K(V_m) = \pi m \varepsilon (x_0 \dot{y}_0 - y_0 \dot{x}_0) \left(1 + \mathcal{O}(\varepsilon + x_0^2 + y_0^2)\right). \tag{20}$$

Proof. Using the chain rule, we rewrite the kinetic energy (11) in the form

$$K(V_m) = -\dot{x}_0 K_x(V_m) - \dot{y}_0 K_y(V_m), \tag{21}$$

where

$$K_x(V_m) = -m\varepsilon^2 \int_{\mathbb{R}^2} \eta_\varepsilon^2 \frac{Y \Psi_m^2}{R^2} \mathrm{d}X\, \mathrm{d}Y,$$

$$K_y(V_m) = m\varepsilon^2 \int_{\mathbb{R}^2} \eta_\varepsilon^2 \frac{X \Psi_m^2}{R^2} \mathrm{d}X\, \mathrm{d}Y.$$

The symmetry of the integrand in $K_x(V_m)$ implies that $K_x(V_m)|_{y_0=0} = 0$. Since η_ε^2 and Ψ_m are smooth with respect to their arguments for small $\varepsilon > 0$, we have $K_x(V_m) = y_0 M_x$, where M_x is smooth for small $(x_0, y_0) \in \mathbb{R}^2$. We write $K_x(V_m) = J_1 + J_2$, where

$$J_1 = -m\varepsilon^2 \int_{\mathbb{R}^2} \eta_\varepsilon^2 \frac{Y(\Psi_m^2 - 1)}{R^2} \mathrm{d}X\, \mathrm{d}Y, \tag{22}$$

$$J_2 = -m\varepsilon^2 \int_{\mathbb{R}^2} \eta_\varepsilon^2 \frac{Y}{R^2} \mathrm{d}X\, \mathrm{d}Y. \tag{23}$$

Because of the behaviour (17), the integrand in J_1 decays like $\mathcal{O}(R^{-3})$ as $R \to \infty$, so that for small $\varepsilon > 0$ and $(x_0, y_0) \in \mathbb{R}^2$, there is $C > 0$ such that

$$|J_1| \leqslant C\varepsilon^2 |y_0|.$$

On the other hand, for any $(x_0, y_0) \in D_0$, the integral in J_2 can be estimated from the sum of two terms,

$$\left| \int_{\mathbb{R}^2 \setminus D_0} \eta_\varepsilon^2 \frac{Y}{R^2} \mathrm{d}x\, \mathrm{d}y \right| \leqslant \varepsilon \int_0^{2\pi} \mathrm{d}\theta \int_1^\infty r\, \mathrm{d}r \frac{\eta_\varepsilon^2 |\sin(\theta)|}{\sqrt{(x-x_0)^2 + (y-y_0)^2}}$$
$$\leqslant C\varepsilon^{1+2/3} |y_0| \int_1^\infty \exp\left(\frac{1-r^2}{2\varepsilon^{2/3}} \right) r\, \mathrm{d}r \leqslant C\varepsilon^{1+4/3} |y_0|$$

and

$$\left| \int_{D_0} \eta_\varepsilon^2 \frac{Y}{R^2} \mathrm{d}x\, \mathrm{d}y \right| \leqslant \varepsilon^2 \int_0^{2\pi} \mathrm{d}\theta \int_0^{\varepsilon^{-1}} \eta_\varepsilon^2 |\sin(\theta)|\, \mathrm{d}R \leqslant C\varepsilon^2 |y_0| \int_0^{\varepsilon^{-1}} \mathrm{d}R \leqslant C\varepsilon |y_0|,$$

where the bounds (5) and (8) have been used. Therefore, for small $\varepsilon > 0$ and $(x_0, y_0) \in \mathbb{R}^2$, there is $C > 0$ such that

$$|J_2| \leqslant C\varepsilon |y_0|.$$

Since $J_2|_{y_0=0} = 0$, we compute

$$\begin{aligned} \partial_{y_0} J_2|_{x_0=y_0=0} &= -m\varepsilon^2 \int_{\mathbb{R}^2} (\partial_y \eta_\varepsilon^2|_{r=\varepsilon R}) \frac{Y}{R^2} \mathrm{d}X\, \mathrm{d}Y \\ &= -m\varepsilon^2 \int_0^{2\pi} \mathrm{d}\theta \int_0^\infty \mathrm{d}R (\partial_r \eta_\varepsilon^2|_{r=\varepsilon R}) \sin^2(\theta) \\ &= \pi m \varepsilon \eta_\varepsilon^2(0) = \pi m \varepsilon + \mathcal{O}(\varepsilon^3), \end{aligned}$$

where the bound (7) is used for the last expansion. Therefore, we obtain

$$K_x(V_m) = \pi m \varepsilon y_0 \left(1 + \mathcal{O}(\varepsilon + x_0^2 + y_0^2)\right).$$

Using similar computations for $K_y(V_m)$, we obtain the expansion (20). ■

3.3. Potential energy

When the variational ansatz (14) is used in the potential energy (12), we obtain

$$\Lambda(V_m) = \varepsilon^2 \int_{\mathbb{R}^2} \eta_\varepsilon^2 \left[\left(\frac{\mathrm{d}\Psi_m}{\mathrm{d}R} \right)^2 + \frac{m^2}{R^2} \Psi_m^2 \right] \mathrm{d}X\, \mathrm{d}Y + \frac{1}{2}\varepsilon^2 \int_{\mathbb{R}^2} \eta_\varepsilon^4 (1 - \Psi_m^2)^2 \mathrm{d}X\, \mathrm{d}Y. \tag{24}$$

The limit $\varepsilon \to 0$ for $\Lambda(V_m)$ is delicate because of the divergence of the integral

$$\int_0^\infty \frac{m^2}{R^2} \Psi_m^2 R\, \mathrm{d}R = \infty.$$

We will prove the following.

Lemma 2. *For small $\varepsilon > 0$ and $(x_0, y_0) \in \mathbb{R}^2$, the potential energy of a single vortex is expanded by*

$$\Lambda(V_m) - \Lambda(V_m)|_{x_0=y_0=0} = -\pi \varepsilon m \omega_m(\varepsilon)(x_0^2 + y_0^2) \left(1 + \mathcal{O}(\varepsilon^{1/3} + x_0^2 + y_0^2)\right), \tag{25}$$

where $\omega_m(\varepsilon)$ is given by

$$\omega_m(\varepsilon) = \varepsilon m \left[1 - 2\log(\varepsilon) + \frac{2}{m^2} \int_0^\infty \left[\left(\frac{\mathrm{d}\Psi_m}{\mathrm{d}R} \right)^2 + \frac{m^2}{R^2} \left(\Psi_m^2 - \frac{R^2}{1+R^2} \right) \right] R\, \mathrm{d}R \right]. \tag{26}$$

Proof. We write $\Lambda(V_m) = I_1 + I_2$, where

$$I_1 = \varepsilon^2 \int_{\mathbb{R}^2} \eta_\varepsilon^2 \left[\left(\frac{\mathrm{d}\Psi_m}{\mathrm{d}R} \right)^2 + \frac{m^2}{R^2} \left(\Psi_m^2 - \frac{R^2}{1+R^2} \right) \right] \mathrm{d}X\,\mathrm{d}Y + \frac{1}{2}\varepsilon^2 \int_{\mathbb{R}^2} \eta_\varepsilon^4 (1-\Psi_m^2)^2 \mathrm{d}X\,\mathrm{d}Y$$

and

$$I_2 = \varepsilon^2 m^2 \int_{\mathbb{R}^2} \frac{\eta_\varepsilon^2}{1+R^2} \mathrm{d}X\,\mathrm{d}Y = \varepsilon^2 m^2 \int_{\mathbb{R}^2} \frac{\eta_\varepsilon^2}{\varepsilon^2 + (x-x_0)^2 + (y-y_0)^2} \mathrm{d}x\,\mathrm{d}y.$$

Because of the behaviour (17), the integrand in I_1 decays like $\mathcal{O}(R^{-4})$ as $R \to \infty$, so that for small $\varepsilon > 0$ and $(x_0, y_0) \in \mathbb{R}^2$, there is $C > 0$ such that

$$|I_1| \leqslant C\varepsilon^2.$$

We can split I_1 into the sum of two terms,

$$I_{10} = \varepsilon^2 \int_{D_\varepsilon(x_0,y_0)} (1 - (x_0+\varepsilon X)^2 - (y_0+\varepsilon Y)^2) \left[\left(\frac{\mathrm{d}\Psi_m}{\mathrm{d}R} \right)^2 + \frac{m^2}{R^2} \left(\Psi_m^2 - \frac{R^2}{1+R^2} \right) \right] \mathrm{d}X\,\mathrm{d}Y$$
$$+ \frac{1}{2}\varepsilon^2 \int_{D_\varepsilon(x_0,y_0)} (1 - (x_0+\varepsilon X)^2 - (y_0+\varepsilon Y)^2)^2 (1-\Psi_m^2)^2 \mathrm{d}X\,\mathrm{d}Y$$

and

$$\Delta I_1 = \varepsilon^2 \int_{\mathbb{R}^2} (\eta_\varepsilon^2 - \eta_0^2) \left[\left(\frac{\mathrm{d}\Psi_m}{\mathrm{d}R} \right)^2 + \frac{m^2}{R^2} \left(\Psi_m^2 - \frac{R^2}{1+R^2} \right) \right] \mathrm{d}X\,\mathrm{d}Y$$
$$+ \frac{1}{2}\varepsilon^2 \int_{\mathbb{R}^2} (\eta_\varepsilon^4 - \eta_0^4)(1-\Psi_m^2)^2\,\mathrm{d}X\,\mathrm{d}Y.$$

Thanks to bound (8) and the fast decay of the integrand, we have $\Delta I_1 = \mathcal{O}(\varepsilon^{2+1/3})$ for small $(x_0, y_0) \in \mathbb{R}^2$. On the other hand, I_{10} can be computed asymptotically as

$$I_{10} = \varepsilon^2 (1 - x_0^2 - y_0^2) \int_{\mathbb{R}^2} \left[\left(\frac{\mathrm{d}\Psi_m}{\mathrm{d}R} \right)^2 + \frac{m^2}{R^2} \left(\Psi_m^2 - \frac{R^2}{1+R^2} \right) \right] \mathrm{d}X\,\mathrm{d}Y$$
$$+ \frac{1}{2}\varepsilon^2 (1 - x_0^2 - y_0^2)^2 \int_{\mathbb{R}^2} (1-\Psi_m^2)^2 \mathrm{d}X\,\mathrm{d}Y + \mathcal{O}(\varepsilon^4 |\log(\varepsilon)|).$$

Combining the two computations and using the constraint (19), we obtain

$$I_1 = 2\pi\varepsilon^2 (1 - x_0^2 - y_0^2) \int_0^\infty \left[\left(\frac{\mathrm{d}\Psi_m}{\mathrm{d}R} \right)^2 + \frac{m^2}{R^2} \left(\Psi_m^2 - \frac{R^2}{1+R^2} \right) \right] R\,\mathrm{d}R$$
$$+ \pi\varepsilon^2 (1 - x_0^2 - y_0^2)^2 m^2 + \mathcal{O}(\varepsilon^{2+1/3}).$$

Note that because η_ε^2 and Ψ_m are smooth in their arguments for any $\varepsilon > 0$, the remainder term in I_1 is smooth for small $(x_0, y_0) \in \mathbb{R}^2$.

The slow decay of the integrand in I_2 renders the asymptotic analysis as $\varepsilon \to 0$ more complicated. For any $(x_0, y_0) \in D_0$, the integral in I_2 can be estimated from the sum of two terms,

$$\int_{\mathbb{R}^2 \setminus D_0} \frac{\eta_\varepsilon^2}{\varepsilon^2 + (x-x_0)^2 + (y-y_0)^2} \mathrm{d}x\,\mathrm{d}y$$
$$\leqslant C\varepsilon^{2/3} \int_0^{2\pi} \mathrm{d}\theta \int_1^\infty r\,\mathrm{d}r \frac{\exp\left(\frac{1-r^2}{2\varepsilon^{2/3}} \right)}{\varepsilon^2 + (x-x_0)^2 + (y-y_0)^2} \leqslant C\varepsilon^{4/3},$$

and

$$\int_{D_0} \frac{\eta_\varepsilon^2 \mathrm{d}x\,\mathrm{d}y}{\varepsilon^2 + (x-x_0)^2 + (y-y_0)^2} \leqslant C \int_0^{2\pi} \mathrm{d}\theta \int_0^{\varepsilon^{-1}} \frac{R\,\mathrm{d}R}{1 + R^2 + R_0^2 - 2R_0 R\cos(\theta - \theta_0)} \leqslant C|\log(\varepsilon)|,$$

where the bounds (5) and (8) have been used and (x_0, y_0) have been represented by

$$x_0 = \varepsilon R_0 \cos(\theta_0), \qquad y_0 = \varepsilon R_0 \sin(\theta_0).$$

Therefore, for small $\varepsilon > 0$ and $(x_0, y_0) \in \mathbb{R}^2$, there is $C > 0$ such that

$$|I_2| \leqslant C\varepsilon^2 |\log(\varepsilon)|.$$

Let $I_2 \equiv I(x_0, y_0)$. We note the symmetry

$$I(-x_0, -y_0) = I(-x_0, y_0) = I(x_0, -y_0) = I(x_0, y_0).$$

Given the nature of the Euler–Lagrange equations, we are not interested in the constant term $I(0, 0)$ but need to derive the quadratic term in the expansion

$$I(x_0, y_0) = I(0, 0) + \tfrac{1}{2}\partial_{x_0}^2 I(0, 0)(x_0^2 + y_0^2) + \mathcal{O}(x_0^2 + y_0^2)^2,$$

where

$$\begin{aligned}\partial_{x_0}^2 I(0,0) &= 2\varepsilon^2 m^2 \int_{\mathbb{R}^2} \eta_\varepsilon^2 \frac{3x^2 - y^2 - \varepsilon^2}{(\varepsilon^2 + x^2 + y^2)^3} \mathrm{d}x\,\mathrm{d}y \\ &= 4\pi m^2 \int_0^\infty \frac{\eta_\varepsilon^2(\varepsilon R)(R^2 - 1)R}{(1 + R^2)^3} \mathrm{d}R \\ &= 4\pi m^2 \left(I_{20} + \Delta I_2\right),\end{aligned}$$

where

$$I_{20} = \int_0^{\varepsilon^{-1}} \eta_\varepsilon^2(\varepsilon R) \frac{(R^2 - 1)R}{(1 + R^2)^3} \mathrm{d}R, \qquad \Delta I_2 = \int_{\varepsilon^{-1}}^\infty \eta_\varepsilon^2(\varepsilon R) \frac{(R^2 - 1)R}{(1 + R^2)^3} \mathrm{d}R.$$

It follows from the bound (5) that $\eta_\varepsilon^2(x) = \mathcal{O}(\varepsilon^{2/3})$ for any $|x| \geqslant 1$. As a result, we have $\Delta I_2 = \mathcal{O}(\varepsilon^{2+2/3})$. To estimate the leading order of I_{20}, we use appendix, where the representation (43) and the asymptotic expansion (44) have been reviewed. Using integration by parts, we obtain

$$\begin{aligned}I_{20} &= \frac{1}{2}\varepsilon^{2+4/3} \int_0^{\varepsilon^{-2/3}} \nu_\varepsilon^2 \frac{1 - \varepsilon^2 - \varepsilon^{2/3} y}{(1 + \varepsilon^2 - \varepsilon^{2/3} y)^3} \mathrm{d}y \\ &= -\frac{1}{2}\varepsilon^{2+2/3} \int_0^{\varepsilon^{-2/3}} \partial_y\left(\nu_\varepsilon^2\right) \frac{1 - \varepsilon^{2/3} y}{(1 + \varepsilon^2 - \varepsilon^{2/3} y)^2} \mathrm{d}y - \frac{\varepsilon^{2+2/3} \nu_\varepsilon^2(0)}{2(1 + \varepsilon^2)^2}.\end{aligned}$$

Because

$$\partial_y\left(\nu_\varepsilon^2\right) = 1 + \mathcal{O}(\varepsilon), \quad y \in [\varepsilon^{-1/3}, \varepsilon^{-2/3}], \qquad \text{as} \quad \varepsilon \to 0,$$

whereas $\nu_\varepsilon^2(0)$ and $\partial_y\left(\nu_\varepsilon^2\right)$ for all $y \in [0, \varepsilon^{-2/3}]$ are bounded as $\varepsilon \to 0$, we can write

$$\begin{aligned}I_{20} &= -\frac{1}{2}\varepsilon^{2+2/3} \int_{\varepsilon^{-1/3}}^{\varepsilon^{-2/3}} \partial_y\left(\nu_\varepsilon^2\right) \frac{1 - \varepsilon^{2/3} y}{(1 + \varepsilon^2 - \varepsilon^{2/3} y)^2} \mathrm{d}y + \mathcal{O}(\varepsilon^{2+1/3}) \\ &= -\frac{1}{2}\varepsilon^{2+2/3} \int_{\varepsilon^{-1/3}}^{\varepsilon^{-2/3}} \frac{1 - \varepsilon^{2/3} y}{(1 + \varepsilon^2 - \varepsilon^{2/3} y)^2} (1 + \mathcal{O}(\varepsilon)) \,\mathrm{d}y + \mathcal{O}(\varepsilon^{2+1/3}) \\ &= \varepsilon^2 \left(\log(\varepsilon) + \frac{1}{2}\right) + \mathcal{O}(\varepsilon^{2+1/3}).\end{aligned}$$

Combining all computations together, we obtain (25) and (26). ■

3.4. The leading-order frequency of vortex precession

Using expansions (20) and (25), we write the linear part of the Euler–Lagrange equations for the averaged Lagrangian $L(V_m) = K(V_m) + \Lambda(V_m)$ in the form

$$-\dot{x}_0 = \omega_m(\varepsilon) y_0, \qquad \dot{y}_0 = \omega_m(\varepsilon) x_0,$$

which means that $\omega_m(\varepsilon)$ is the eigenfrequency of oscillations of the single vortex of charge m in the harmonic potential in the large-density limit $\varepsilon \to 0$.

When $\varepsilon = \frac{1}{2\mu}$ and $\Omega_m(\mu) = \frac{1}{2}\omega_m(\varepsilon)$ are used for the original Gross–Pitaevskii equation (1), we can write the eigenfrequency of the vortex precession for $m = 1$ and $m = 2$ in the form

$$\Omega_1(\mu) = \frac{1}{2\mu} \log(A_1 \mu), \qquad \Omega_2(\mu) = \frac{1}{\mu} \log(A_2 \mu), \tag{27}$$

where

$$A_m = 2 \exp\left[\frac{1}{m^2} \int_0^\infty \left[\left(\frac{\mathrm{d}\Psi_m}{\mathrm{d}R} \right)^2 + \frac{m^2}{R^2} \left(\Psi_m^2 - \frac{R^2}{1+R^2} \right) \right] R \, \mathrm{d}R + \frac{1}{2} \right], \qquad m = 1, 2.$$

Using the numerical approximations of the integrals from the results of the shooting method in figure 1, we obtain

$$A_1 \approx 2.7047, \qquad A_2 \approx 1.089.$$

The numerically fitted value for the constant A_1 was found in [20] to be

$$A_1^{\text{num}} \approx 2\sqrt{2}\pi \approx 8.8858.$$

Although the numerically fitted constant shows a better agreement for smaller values of μ, we emphasize that the constant A_1 is derived in the opposite limit $\mu \to \infty$ using the vortex solution (14) of the defocusing nonlinear Schrödinger equation (13).

Figure 2 shows the results of numerical approximations of vortices for $m = 1$ (left) and $m = 2$ (right). The numerical method is the same as the one used by Middelkamp *et al* in [20, 21]. For technical reasons, the numerical results have been obtained for the harmonic potential of the form

$$V(x, y) = \frac{\Omega^2}{2}(x^2 + y^2), \qquad \Omega = 0.2,$$

and both the eigenfrequencies and the chemical potential have been rescaled by Ω; such a rescaling absorbs the dependence on the trap frequency Ω.

Figure 2 shows the imaginary parts λ_i of the relevant eigenvalues λ as a function of the chemical potential μ. The asymptotic approximations (27) are shown by the (green) dashed–dotted line for the lowest eigenfrequency that corresponds to the vortex precession near the centre of the harmonic potential. In addition to this eigenfrequency (often referred to as the *anomalous mode* in the physical literature [3]), there exist other eigenfrequencies that correspond to the oscillations of the ground state. The latter eigenfrequencies in the space of two and three dimensions have recently been studied asymptotically and numerically in our work [15].

In the case of the $m = 1$ vortex, the (red) solid line in figure 2 (left) shows the numerical fit of [20] with the constant A_1^{num}. Although the variational result with the simple vortex ansatz (14) considered herein clearly fails to capture the eigenfrequency for small values of the chemical potential (i.e. for small atom numbers or away from the large-density limit), it can be straightforwardly seen to have the correct functional dependence on μ. Furthermore,

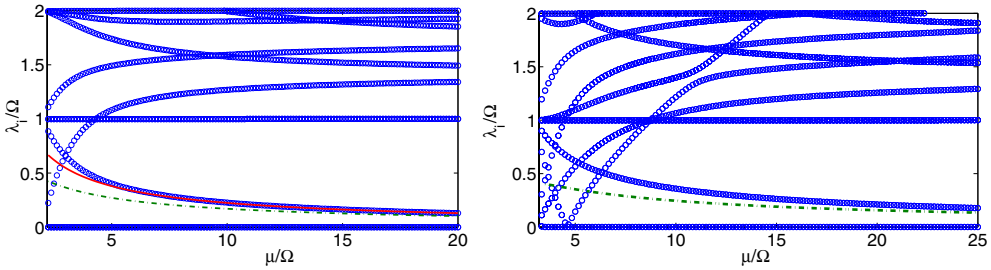

Figure 2. Numerical approximation of eigenfrequencies for a single vortex with $m = 1$ (left) and $m = 2$ (right). The imaginary part λ_i of the eigenvalues is shown as a function of the chemical potential μ. The numerically obtained eigenvalues are shown by (blue) circles, while the analytical predictions (27) are given by (green) dashed–dotted line. The (red) solid line on the left figure indicates the prediction (27) with $A_1 \equiv A_1^{\text{num}}$.

the variational approximation becomes increasingly more accurate for larger values of the chemical potential.

In the case of the $m = 2$ vortex, in addition to the vortex precession frequencies and the frequencies of oscillations of the ground state, there is another higher eigenfrequency, which may cause instabilities due to collisions with eigenfrequencies of the ground state. These instabilities were originally explored in [30] and more recently analysed numerically in [18]. This eigenfrequency of a dynamically unstable mode cannot be captured within the present variational method.

4. Dipole

We shall now consider the dipole configuration of a vortex located at (x_0, y_0) and an antivortex located at $(-x_0, y_0)$ on the plane $(x, y) \in \mathbb{R}^2$. The dipole configuration has the zero total vortex charge. For $y_0 = 0$, this configuration is symmetric relative to the harmonic potential and can be rotated on the (x, y) plane at any angle. To remove this rotational degree of freedom, we shift the vortex–antivortex pair in the same direction relative to the y-axis. Similar configurations were considered in [19, 22] and more recently in [21].

Because single vortices of charge m are spectrally unstable for $m \geqslant 2$ in some intervals of values of ε, we shall only consider the dipole consisting of charge-one vortices.

4.1. Free dipole

Let us write the charge-one vortex placed at the point $(x_0, y_0) \in \mathbb{R}^2$ as

$$V_1(x - x_0, y - y_0) = \Psi_1(R)e^{i\theta},$$

where (R, θ) are polar coordinates (the same coordinates are used in section 3). We consider the variational ansatz

$$V_d(x, y) = V_1(x - x_0, y - y_0)\bar{V}_1(x + x_0, y - y_0). \tag{28}$$

We shall use variables

$$x = \varepsilon X, \qquad y = y_0 + \varepsilon Y, \qquad x_0 = \varepsilon A, \qquad y_0 = \varepsilon B, \tag{29}$$

We note that

$$\left|\frac{\partial V_d}{\partial X}\right|^2 + \left|\frac{\partial V_d}{\partial Y}\right|^2 = \mathcal{O}(R^{-4}) \quad (1 - |V_d|^2)^2 = \mathcal{O}(R^{-4}) \qquad \text{as} \quad R \to \infty, \tag{30}$$

where $R = \sqrt{X^2 + Y^2}$. Note that the weaker decay $\mathcal{O}(R^{-2})$ of the first term in (30) holds for the single vortex. However, the weaker decay of individual vortices is compensated in the vortex–antivortex pair with the zero total charge.

Computing the potential energy (12) for $v = V_d$ and $\eta_\varepsilon \equiv 1$, we obtain

$$\Lambda_R(V_d) = \int_{\mathbb{R}^2} \left(\left| \frac{\partial V_d}{\partial X} \right|^2 + \left| \frac{\partial V_d}{\partial Y} \right|^2 + \frac{1}{2}(1 - |V_d|^2)^2 \right) \mathrm{d}X\, \mathrm{d}Y,$$

where $\Lambda_R(V_d)$ is scaled by ε^2 compared with $\Lambda(V)$.

Thanks to the fast decay of the integrands given by (30), the double integral converges for any finite $A > 0$. However, it does not exclude a growth of $\Lambda_R(V_d)$ as $A \to \infty$. It was justified by Ovchinnikov and Sigal [24] that the growth of $\Lambda_R(V_d)$ is logarithmic and, more precisely, adjusted to our notations, we have

$$\Lambda_R(V_d) = 2\pi \log(A) + \mathcal{O}(1) \qquad \text{as} \quad A \to \infty. \tag{31}$$

The interaction energy is referred as the logarithmic Kirchhoff–Onsager energy [24, 25]. It behaves similarly to the one for vortices in fluid mechanics [4].

4.2. Potential energy

We will prove the following.

Lemma 3. *For small $\varepsilon > 0$ and $(x_0, y_0) \in \mathbb{R}^2$ such that x_0/ε is large as $\varepsilon \to 0$, the potential energy of a dipole is expanded by*

$$\Lambda(V_d) - \Lambda(V_d)|_{x_0=y_0=0} = 4\pi\varepsilon^2(x_0^2 + y_0^2)\,(\log(\varepsilon) + \mathcal{O}(1)) + 2\pi\varepsilon^2\,(\log(x_0/\varepsilon) + \mathcal{O}(1))\,. \tag{32}$$

Proof. We substitute the variational ansatz (28) to the potential energy (12) and rewrite it as a sum of three terms

$$\Lambda(V_d) = \Lambda(V_1^+) + \Lambda(\bar{V}_1^-) + \Lambda_{\text{over}}(V_1^+, V_1^-),$$

where $V_1^\pm(x, y) = V_1(x \mp x_0, y - y_0)$ and Λ_{over} contains the overlapping terms

$$\begin{aligned}\Lambda_{\text{over}}(V_1^+, V_1^-) = {} & \varepsilon^2 \int_{\mathbb{R}^2} \eta_\varepsilon^2 \left[|\nabla V_1^+|^2 (|V_1^-|^2 - 1) + |\nabla V_1^-|^2 (|V_1^+|^2 - 1) \right] \mathrm{d}x \\ & + \varepsilon^2 \int_{\mathbb{R}^2} \eta_\varepsilon^2 \left[\bar{V}_1^+ \bar{V}_1^- (\nabla V_1^+ \cdot \nabla V_1^-) + (\nabla \bar{V}_1^+ \cdot \nabla \bar{V}_1^-) V_1^+ V_1^- \right] \mathrm{d}x \\ & + \frac{1}{2}\varepsilon^2 \int_{\mathbb{R}^2} \eta_\varepsilon^4 \left[(1 - |V_1^+|^2 |V_1^-|^2)^2 - (1 - |V_1^+|^2)^2 - (1 - |V_1^-|^2)^2 \right] \mathrm{d}x.\end{aligned}$$

We are only interested in capturing the leading-order terms which grow logarithmically as $\varepsilon \to 0$, $A \to \infty$, and $x_0 = \varepsilon A \to 0$. By lemma 2, we know that

$$\Lambda(V_1^\pm) - \Lambda(V_1^\pm)|_{x_0=y_0=0} = 2\pi\varepsilon^2(x_0^2 + y_0^2)\,(\log(\varepsilon) + \mathcal{O}(1))\,. \tag{33}$$

On the other hand, $\Lambda(V_d)$ is written in variables (29) as

$$\Lambda(V_d) = \varepsilon^2 \int_{\mathbb{R}^2} \eta_\varepsilon^2 \left(\left| \frac{\partial V_d}{\partial X} \right|^2 + \left| \frac{\partial V_d}{\partial Y} \right|^2 \right) \mathrm{d}X\, \mathrm{d}Y + \frac{1}{2}\varepsilon^2 \int_{\mathbb{R}^2} \eta_\varepsilon^4 (1 - |V_d|^2)^2 \mathrm{d}X\, \mathrm{d}Y.$$

Thanks to the bound (8) and the fast decay of the integrands given by (30), for small $\varepsilon > 0$ and any $(A, B) \in \mathbb{R}^2$, there is $C > 0$ such that

$$|\Lambda(V_d)| \leqslant C\varepsilon^2.$$

Note that the $\log(\varepsilon)$ in expansion (33) goes to the order $\mathcal{O}(\varepsilon^4|\log(\varepsilon)|)$ when the variables (29) are used. From expansion (31) for the interaction energy, we conclude that

$$\Lambda_{\text{over}}(V_1^+, V_1^-) = 2\pi\varepsilon^2\left(\log(x_0/\varepsilon) + \mathcal{O}(1)\right), \qquad \text{as} \quad x_0/\varepsilon \to \infty, \quad x_0 \to 0. \tag{34}$$

Expansions (33) and (34) imply (32). ■

4.3. Kinetic energy

We will prove the following.

Lemma 4. *For small $\varepsilon > 0$ and $(x_0, y_0) \in \mathbb{R}^2$, the kinetic energy of a dipole is expanded by*

$$K(V_d) = 2\pi\varepsilon(x_0\dot{y}_0 - y_0\dot{x}_0)\left(1 + \mathcal{O}(\varepsilon + x_0^2 + y_0^2)\right). \tag{35}$$

Proof. We substitute the variational ansatz (28) to the kinetic energy (11) and rewrite it as a sum of three terms

$$K(V_d) = K(V_1^+) + K(\bar{V}_1^-) + K_{\text{over}}(V_1^+, V_1^-),$$

where the overlapping kinetic energy is

$$K_{\text{over}}(V_1^+, V_1^-) = \frac{\mathrm{i}}{2}\varepsilon\int_{\mathbb{R}^2}\eta_\varepsilon^2\left[(V_1^+(\bar{V}_1^+)_t - \bar{V}_1^+(V_1^+)_t)(|V_1^-|^2 - 1)\right.$$
$$\left.+(\bar{V}_1^-(V_1^-)_t - V_1^-(\bar{V}_1^-)_t)(|V_1^+|^2 - 1)\right]\mathrm{d}x$$

By lemma 1, we know that

$$K(V_1^\pm) = \pi\varepsilon(x_0\dot{y}_0 - y_0\dot{x}_0)\left(1 + \mathcal{O}(\varepsilon + x_0^2 + y_0^2)\right). \tag{36}$$

On the other hand, the kinetic energy is written in variables (29) as

$$K(V_d) = \dot{A}K_A(V_d) - \dot{B}K_B(V_d),$$

where

$$K_A(V_d) = \frac{\mathrm{i}}{2}\varepsilon^3\int_{\mathbb{R}^2}\eta_\varepsilon^2(x)(V_d\partial_A\bar{V}_d - \bar{V}_d\partial_A V_d)\,\mathrm{d}X\,\mathrm{d}Y,$$
$$K_B(V_d) = \frac{\mathrm{i}}{2}\varepsilon^3\int_{\mathbb{R}^2}\eta_\varepsilon^2(x)(V_d\partial_Y\bar{V}_d - \bar{V}_d\partial_Y V_d)\,\mathrm{d}X\,\mathrm{d}Y.$$

We have

$$(V_d\partial_A\bar{V}_d - \bar{V}_d\partial_A V_d) = \mathcal{O}(R^{-3}), \qquad (V_d\partial_Y\bar{V}_d - \bar{V}_d\partial_Y V_d) = \mathcal{O}(R^{-2}), \qquad \text{as} \quad R \to \infty. \tag{37}$$

Because of the sufficiently strong decay in the first asymptotic expansion (37), for small $\varepsilon > 0$ and any $(A, B) \in \mathbb{R}^2$, there is $C > 0$ such that

$$|K_A(V_d)| \leqslant C\varepsilon^3|B|.$$

The second asymptotic expansion (37) does not decay fast enough, which may be troublesome. However, we note that we are interested in this term only for $B = 0$, in which case the symmetry of the integrand can be used to conclude that

$$\frac{\mathrm{i}}{2}\int_0^{2\pi}(V_d\partial_Y\bar{V}_d - \bar{V}_d\partial_Y V_d)\Big|_{B=0}\mathrm{d}\theta = \mathcal{O}(R^{-4}).$$

As a result, for small $\varepsilon > 0$ and any $(A, B) \in \mathbb{R}^2$, there is $C > 0$ such that

$$|K_B(V_d)| \leqslant C\varepsilon^3|A|.$$

Therefore, $K_{\rm over}(V_1^+, V_1^-)$ may only diverge as $x_0/\varepsilon \to \infty$ and $\varepsilon \to 0$ at the order of ε^3. This consideration together with expansion (36) imply (35). ■

4.4. The leading-order frequency of dipole oscillations

Truncating the asymptotic expansions (32) and (35) at the leading order, we write the averaged Lagrangian $L(V_d) = K(V_d) + \Lambda(V_d)$ in the form

$$L(V_d) = 2\pi\varepsilon(x_0\dot{y}_0 - y_0\dot{x}_0) + 4\pi\varepsilon^2\log(\varepsilon)(x_0^2 + y_0^2) + 2\pi\varepsilon^2\log(x_0/\varepsilon). \tag{38}$$

The Euler–Lagrange equations generated by $L(V_d)$ yield the system,

$$\dot{y}_0 + 2\varepsilon\log(\varepsilon)x_0 + \frac{\varepsilon}{2x_0} = 0,$$
$$-\dot{x}_0 + 2\varepsilon\log(\varepsilon)y_0 = 0.$$

The equilibrium state of this system corresponds to

$$x_0 = \frac{1}{2|\log(\varepsilon)|^{1/2}}, \qquad y_0 = 0,$$

which shows that $x_0 \to 0$ and $A = x_0/\varepsilon \to \infty$ as $\varepsilon \to 0$. This verifies *a posteriori* the assumptions in the derivation of the averaged Lagrangian (38).

The linearized dynamics near the equilibrium state is an oscillation with the squared frequency

$$\omega_d^2(\varepsilon) = 8\varepsilon^2\log^2(\varepsilon).$$

Recall that the frequency of the vortex precession for the charge-one vortex is

$$\omega_1(\varepsilon) = 2\varepsilon|\log(\varepsilon)| + \mathcal{O}(\varepsilon) \qquad \text{as} \quad \varepsilon \to 0.$$

Therefore, $\omega_d(\varepsilon) \approx \sqrt{2}\omega_1(\varepsilon)$ up to the terms of the order of $\mathcal{O}(\varepsilon)$.

Figure 3 showcases a prototypical example of the vortex dipole, both in terms of the solution profile (the solution amplitude and phase in the top panels), but also in terms of the linearization spectrum (real and imaginary parts of the eigenvalues in the bottom panels). Compared with the eigenfrequencies of oscillations of the ground state, the linearization spectrum possesses a higher multiplicity of the zero eigenvalue due to the invariance of the dipole location under the effect of rotation. It additionally possesses a non-zero eigenvalue which, upon collision with an eigenvalue bifurcating from the origin, gives rise to a complex eigenvalue instability, as is evident in the bottom panels of figure 3 for $3.9 < \mu/\Omega < 4.4$. Once again, the agreement of the lowest order analytical prediction with the lowest imaginary eigenvalue of the system is progressively improved, as the large-density limit is approached. The above frequency corresponds to an epicyclic precession of the vortex–antivortex pair around their equilibrium location.

5. Quadrupole

We shall now consider the quadrupole configuration consisting of two charge-one vortices placed at $\boldsymbol{x}_1 = (x_1, y_1)$ and $\boldsymbol{x}_3 = (-x_3, -y_3)$ and two charge-one antivortices placed at $\boldsymbol{x}_2 = (-x_2, y_2)$ and $\boldsymbol{x}_4 = (x_4, -y_4)$, where all x_j and y_j are assumed to be positive. The quadrupole configuration is symmetric if

$$x_j = y_j = x_0 > 0, \qquad 1 \leqslant j \leqslant 4. \tag{39}$$

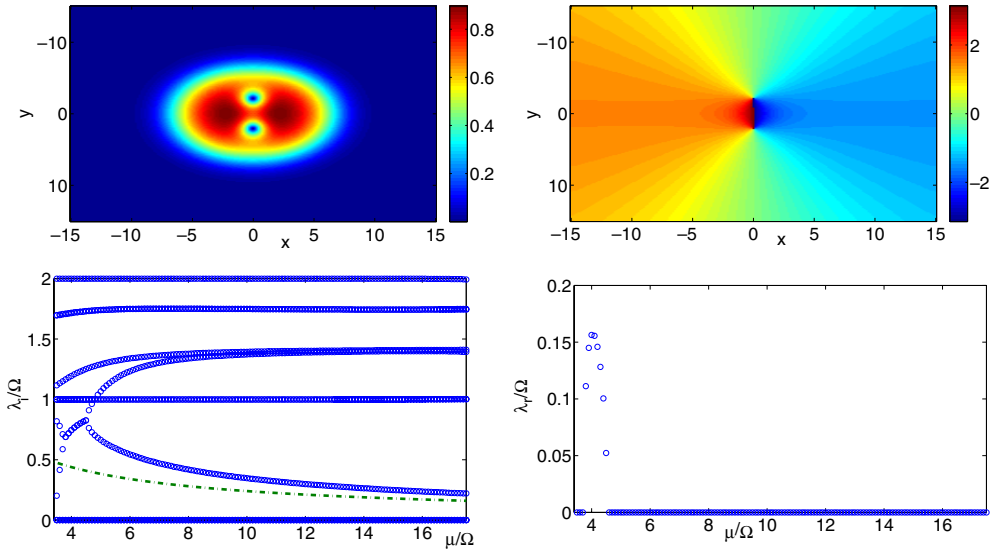

Figure 3. The top panels show a prototypical example of the dipole configuration for $\mu/\Omega = 5$; the amplitude is shown on the left and corresponding phase on the right. The bottom panels show the imaginary (left) and real (right) parts of the relevant eigenfrequencies. The (green) dashed–dotted line corresponds to the analytical result, which progressively improves its approximation of the numerical result, as μ is increased. The oscillatory instability associated with a complex eigenvalue quartet emerges from the collision of two eigenvalue pairs, in the vicinity of $\mu/\Omega \approx 4$.

The quadrupole configuration has the zero total vortex charge and can be rotated on the (x, y) plane at any angle. Similar configurations were considered in [19, 22] and more recently in [21].

We adopt the variational ansatz

$$V_q(x, y) = V_1(x - x_1, y - y_1)\bar{V}_1(x + x_2, y - y_2)V_1(x + x_3, y + y_3)\bar{V}_1(x - x_4, y + y_4), \tag{40}$$

where V_1 is the charge-one vortex. Similarly to our treatment of the multi-soliton case in [5], we will construct the averaged Lagrangian $L(V_q)$ ad hoc, based on the approximations of the previous two sections.

Combining the computations of the averaged Lagrangian for individual vortices and their effective interaction energy, we obtain

$$L(V_q) = \pi\varepsilon \sum_{1\leqslant i\leqslant 4} (x_j\dot{y}_j - y_j\dot{x}_j) + 2\pi\varepsilon^2 \log(\varepsilon) \sum_{1\leqslant i\leqslant 4} (x_j^2 + y_j^2) + 2\pi\varepsilon^2 \sum_{1\leqslant i<j\leqslant 4} \log|\boldsymbol{x}_i - \boldsymbol{x}_j|, \tag{41}$$

where we note that the difference in signs in front of x_j and y_j is cancelled because of the difference in the charge signs for individual vortices. The Euler–Lagrange equations generated by $L(V_q)$ yield the system,

$$\dot{y}_1 + 2\varepsilon \log(\varepsilon)x_1 + \frac{\varepsilon(x_1 + x_2)}{(x_1 + x_2)^2 + (y_1 - y_2)^2} + \frac{\varepsilon(x_1 - x_4)}{(x_1 - x_4)^2 + (y_1 + y_4)^2} + \frac{\varepsilon(x_1 + x_3)}{(x_1 + x_3)^2 + (y_1 + y_3)^2} = 0,$$

$$-\dot{x}_1 + 2\varepsilon \log(\varepsilon) y_1 + \frac{\varepsilon(y_1 - y_2)}{(x_1 + x_2)^2 + (y_1 - y_2)^2} + \frac{\varepsilon(y_1 + y_4)}{(x_1 - x_4)^2 + (y_1 + y_4)^2} + \frac{\varepsilon(y_1 + y_3)}{(x_1 + x_3)^2 + (y_1 + y_3)^2} = 0,$$

as well as three more pairs of equations, which can be obtained by the rotational symmetry.

The symmetric quadrupole configuration (39) is found from a scalar equation

$$2\log(\varepsilon)x_0 + \frac{1}{2x_0} + \frac{1}{4x_0} = 0 \Rightarrow x_0 = \left(\frac{3}{8|\log(\varepsilon)|}\right)^{1/2}.$$

Note that if the quadrupole configuration is rotated to the one with the four vortices located at $(x_0^*, 0)$, $(0, x_0^*)$, $(-x_0^*, 0)$, and $(0, -x_0^*)$, then $x_0^* = \sqrt{2}x_0 = \frac{\sqrt{3}}{2|\log(\varepsilon)|^{1/2}}$.

Routine computations of the linearized system show that the linearized dynamics near the equilibrium state is given by the system of equations

$$\begin{aligned} L\boldsymbol{x} + M\boldsymbol{y} &= -\mathrm{i}\lambda\boldsymbol{y}, \\ M\boldsymbol{x} + L\boldsymbol{y} &= \mathrm{i}\lambda\boldsymbol{x}, \end{aligned} \tag{42}$$

where

$$L = \begin{bmatrix} 6 & 2 & 0 & 2 \\ 2 & 6 & 2 & 0 \\ 0 & 2 & 6 & 2 \\ 2 & 0 & 2 & 6 \end{bmatrix}, \qquad M = \begin{bmatrix} 1 & 0 & 1 & 0 \\ 0 & 1 & 0 & 1 \\ 1 & 0 & 1 & 0 \\ 0 & 1 & 0 & 1 \end{bmatrix}, \qquad \lambda = \frac{3\omega_q(\varepsilon)}{\varepsilon|\log(\varepsilon)|}.$$

Computing eigenvalues of the matrix eigenvalue problem (42), we obtain a double zero, a pair of eigenvalues $\pm 4\sqrt{6}$, and a double pair of eigenvalues ± 6. As a result, we obtain the squared frequencies of the three quadrupole oscillations

$$\begin{aligned} \omega_q^2(\varepsilon) &= 4\varepsilon^2 \log^2(\varepsilon), \\ \omega_q^2(\varepsilon) &= 4\varepsilon^2 \log^2(\varepsilon), \\ \omega_q^2(\varepsilon) &= \frac{32}{3}\varepsilon^2 \log^2(\varepsilon), \end{aligned}$$

and a double zero eigenvalue corresponding to the rotational degree of freedom. Recall that the precession frequency of the charge-one vortex is

$$\omega_1(\varepsilon) = 2\varepsilon|\log(\varepsilon)| + \mathcal{O}(\varepsilon) \qquad \text{as} \quad \varepsilon \to 0.$$

We have thus obtained two quadrupole modes with $\omega_q(\varepsilon) \approx \omega_1(\varepsilon)$ and one quadrupole mode with $\omega_q(\varepsilon) \approx \frac{2\sqrt{2}}{\sqrt{3}}\omega_1(\varepsilon)$ as $\varepsilon \to 0$.

Figure 4 shows a prototypical example of the vortex quadrupole. The spectrum of eigenvalues includes three imaginary pairs of eigenvalues (corresponding to the above 'anomalous modes') in addition to eigenfrequencies of the ground state, as well as the higher multiplicity of the zero eigenvalue due to the rotational freedom of the quadrupole on the plane. Two smaller non-zero eigenvalues are close to the precession frequency $\omega_1(\varepsilon)$ of the single charge-one vortex, while the larger imaginary eigenvalue pair is closer to the frequency $\omega_q(\varepsilon) \approx \frac{2\sqrt{2}}{\sqrt{3}}\omega_1(\varepsilon)$. We note that the vortex quadrupole is unstable in a parametric interval of $4.1 < \mu/\Omega < 7.4$ due to collisions of the eigenvalue bifurcating from the origin and the larger eigenvalue. The instability band is finite and the larger eigenvalue becomes purely imaginary again but slightly higher than the asymptotic result shown by the corresponding (green) dashed–dotted line. As in the previous cases considered, the relevant discrepancy tends to disappear in the limit of large chemical potential μ.

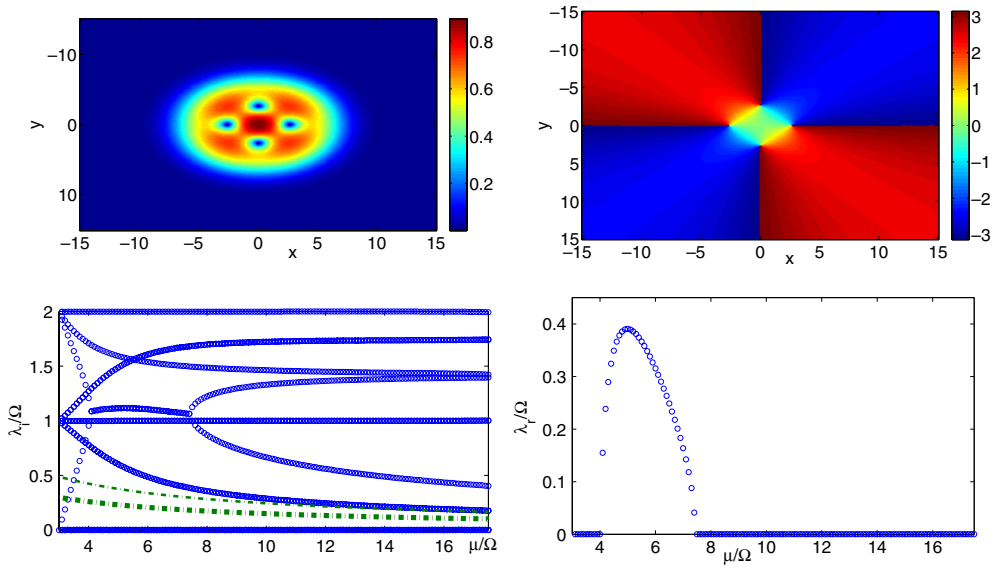

Figure 4. Same as figure 3, but for a vortex quadrupole. In this case, in the bottom left panel, the (green) thicker and thinner dash-dotted lines represent, respectively, the frequencies $\omega(\varepsilon) = \omega_1(\varepsilon)$ (double) and $\omega(\varepsilon) = 2\sqrt{2}\omega_1(\varepsilon)/\sqrt{3}$, which are the internal eigenfrequencies of the quadrupole. The real part of the unstable eigenvalue quartet is shown in the bottom right panel.

6. Conclusion

The aim of this work was to establish the Rayleigh–Ritz variational method as a relevant tool in examining the precessional dynamics of vortices in harmonic potentials, inspired by the intense recent attention that this subject has received in the physics community. In the case of a single vortex, the variational approximation was shown to lead to the correct asymptotic dependence of the precession frequency on the chemical potential. A deficiency of our approach is that it solely captures the precession mode of the vortex dynamics, but cannot account for other eigenmodes that in appropriate ranges of chemical potentials lead to the dynamical instability and splitting of the vortices of a higher topological charge into the ones of a lower charge [12, 30].

The case of dipole and quadrupole configurations is somewhat more intricate, as a more elaborate variational approximation takes into account the individual vortices and their respective charges and locations. An additional complicating factor in that case is again the dynamical instabilities upon collisions of eigenfrequencies associated with the vortex motion and the eigenfrequencies associated with oscillations of the ground state. The collisions between eigenvalues that lead to instabilities appear to affect the 'eigenvalue trajectories' as a function of the chemical potential and could therefore influence the quality of the match to the variational predictions. Nevertheless, we have observed the relevant predictions to approach asymptotically their numerically obtained counterparts for larger chemical potentials.

From the perspective of multiple vortex configurations, it is interesting to generalize the variational approach to different numbers of vortices. The case of three vortices with either two of the same charge and one of opposite (which are typically found to be aligned), as well as that of all three vortices bearing the same charge (in which case they are typically found to form an equilateral triangle which is expected to be rigidly rotating) already constitute

an intriguing case that has experimentally been explored in [31] and awaits a corresponding theoretical investigation. On the other hand, just as one has two and four vortex configurations, it is entirely natural to expect that six or eight vortex states of alternating charges populating the vertices of a hexagonal or octagonal pattern. Developing a more general variational theory for such vortex configurations of zero net charge (or for that matter for complexes of numerous vortices of a single type of charge, or even for the more exotic states intermediate between the above two) would be an interesting endeavor for future investigations.

Acknowledgments

DEP is partially supported by the NSERC grant. PGK is partially supported by NSF-DMS-0349023 (CAREER), NSF-DMS-0806762 and the Alexander-von-Humboldt Foundation. DEP thanks M Coles, S Gustafson, and R Kollar for useful discussions.

Appendix. Justification of the uniform bound (8)

To clarify the proof of bound (8), we follow the asymptotic analysis in [11].

Let η_ε be written in the equivalent form

$$\eta_\varepsilon(x) = \varepsilon^{1/3} v_\varepsilon(y), \qquad y = \frac{1-|x|^2}{\varepsilon^{2/3}}, \tag{43}$$

where v_ε solves

$$4(1-\varepsilon^{2/3}y)v_\varepsilon''(y) - 4\varepsilon^{2/3}v_\varepsilon'(y) + yv_\varepsilon(y) - v_\varepsilon^3(y) = 0, \qquad y \in (-\infty, \varepsilon^{-2/3}).$$

Let v_0 be the unique solution of the Painlevé-II equation

$$4v_0''(y) + yv_0(y) - v_0^3(y) = 0, \qquad y \in \mathbb{R},$$

such that $v_0(y) = y^{1/2} + \mathcal{O}(y^{-5/2})$ as $y \to \infty$ and $v_0(y)$ decays to zero as $y \to -\infty$ faster than any exponential function. By theorem 1 in [11], v_ε is a $\mathcal{C}^\infty$ function on $(-\infty, \varepsilon^{-2/3}]$, which is expanded into the asymptotic series for any fixed $N \geqslant 0$:

$$v_\varepsilon(y) = \sum_{n=0}^{N} \varepsilon^{2n/3} v_n(y) + \varepsilon^{2(N+1)/3} R_{N,\varepsilon}(y), \tag{44}$$

where $\{v_n\}_{n=1}^N$ are uniquely defined ε-independent functions on $\mathbb{R}$ and $R_{N,\varepsilon}(y)$ is the remainder term on $(-\infty, \varepsilon^{-2/3}]$.

Let $U_{N,\varepsilon}(z) = R_{N,\varepsilon}(\varepsilon^{-2/3} - \varepsilon^{2/3}|z|^2)$ be defined on $\mathbb{R}^2$. It was proved in [11] that there is $C_N > 0$ for small $\varepsilon > 0$ such that

$$\|U_{N,\varepsilon}\|_{H^2} \leqslant C_N \varepsilon^{-1/3}. \tag{45}$$

Recall that $H^2(\mathbb{R}^2)$ is embedded into $L^\infty(\mathbb{R}^2)$. The error estimate (8) follows from representation (43), expansion (44) for any $N \geqslant 0$, bound (45) and $\sup_{y\in\mathbb{R}^+} |v_0(y) - y^{1/2}| < \infty$.

References

[1] Bethuel F, Brezis H and Hélein F 1994 *Ginzburg-Landau Vortices* (*Progress in Nonlinear Differential Equations and their Applications* vol 13) (Boston, MA: Birkhäuser)

[2] Brezis H, Merle F and Riviére T 1994 Quantization effects for $-\Delta u = u(1-|u|^2)$ in $\boldsymbol{R}^2$ *Arch. Rational Mech. Anal.* **126** 35–58

[3] Carretero-González R, Frantzeskakis D J and Kevrekidis P G 2008 Nonlinear waves in Bose–Einstein condensates: physical relevance and mathematical techniques *Nonlinearity* **21** R139–R202

[4] Chorin A J and Marsden J E 1993 *A Mathematical Introduction to Fluid Mechanics* (New York: Springer)
[5] Coles M P, Pelinovsky D E and Kevrekidis P G 2010 Excited states in the large-density limit: a variational approach *Nonlinearity* **23** 1753–70
[6] Crasovan L-C, Vekslerchik V, Pérez-García V M, Torres J P, Mihalache D and Torner L 2003 Stable vortex dipoles in nonrotating Bose-Einstein condensates *Phys. Rev.* A **68** 063609
[7] Di Menza L 2009 Numerical computation of solitons for optical systems *Math. Modelling Numer. Anal.* **43** 173–208
[8] Fetter A L 2009 Rotating trapped Bose–Einstein condensates *Rev. Mod. Phys.* **81** 647–91
[9] Fetter A L and Svidzinksy A A 2001 Vortices in a trapped dilute Bose–Einstein condensate *J. Phys.: Condens. Matter* **13** R135–94
[10] Freilich D V, Bianchi D M, Kaufman A M, Langin T K and Hall D S 2010 Real-time dynamics of single vortex lines and vortex dipoles in a Bose–Einstein condensate *Science* **329** 1182–5
[11] Gallo C and Pelinovsky D 2009 On the Thomas–Fermi ground state in a radially symmetric parabolic trap arXiv:0911.3913v1
[12] Herring G, Carr L D, Carretero-González R, Kevrekidis P G and Frantzeskakis D J 2008 Radially symmetric nonlinear states of harmonically trapped Bose–Einstein condensates *Phys. Rev.* A **77** 023625
[13] Ignat R and Millot V 2006 The critical velocity for vortex existence in a two-dimensional rotating Bose–Einstein condensate *J. Funct. Anal.* **233** 260–306
[14] Ignat R and Millot V 2006 Energy expansion and vortex location for a two-dimensional rotating Bose–Einstein condensate *Rev. Math. Phys.* **18** 119–62
[15] Kevrekidis P G and Pelinovsky D E 2010 Distribution of eigenfrequencies for oscillations of the ground state in the Thomas–Fermi limit *Phys. Rev.* A **81** 023627
[16] Kivshar Yu S, Christou J, Tikhonenko V, Luther-Davies B and Pismen L M 1998 Dynamics of optical vortex solitons *Opt. Commun.* **152** 198–206
[17] Klein A, Jaksch D, Zhang Y and Bao W 2007 Dynamics of vortices in weakly interacting Bose–Einstein condensates *Phys. Rev.* A **76** 043602
[18] Kollar R and Pego R L 2011 Spectral stability of vortices in two-dimensional Bose–Einstein condensates via the Evans function and Krein signature arXiv:1103.0157v1
[19] Li W, Haque M and Komineas S 2008 Vortex dipole in a trapped two-dimensional Bose–Einstein condensate *Phys. Rev.* A **77** 053610
[20] Middelkamp S, Kevrekidis P G, Frantzeskakis D J, Carretero–Gonzalez R and Schmelcher P 2010 Anomalous modes and matter-wave vortices in the presence of collisional inhomogeneities and finite temperature *J. Phys. B: At. Mol. Opt. Phys.* **43** 155303
[21] Middelkamp S, Kevrekidis P G, Frantzeskakis D J, Carretero–Gonzalez R and Schmelcher P 2010 Bifurcations, stability, and dynamics of multiple matter-wave vortex states *Phys. Rev.* **82** 013646
[22] Möttönen M, Virtanen S M M, Isoshima T and Salomaa M M 2005 Stationary vortex clusters in nonrotating Bose–Einstein condensates *Phys. Rev.* A **71** 033626
[23] Neely T W, Samson E C, Bradley A S, Davis M J and Anderson B P 2010 Observation of vortex dipoles in an oblate Bose–Einstein condensate *Phys. Rev. Lett.* **104** 160401
[24] Ovchinnikov Y N and Sigal I M 2002 The energy of Ginzburg–Landau vortices *Euro. J. Appl. Math.* **13** (2) 153–78
[25] Ovchinnikov Y N and Sigal I M 2004 Symmetry-breaking solutions of the Ginzburg–Landau equation *JETP* **99** 1090–107
[26] Pelinovsky D 2010 Asymptotic properties of excited states in the Thomas–Fermi limit *Nonlinear Analysis* **73** 2631–43
[27] Pethick C J and Smith H 2002 *Bose–Einstein Condensation in Dilute Gases* (Cambridge: Cambridge University Press)
[28] Pismen L M 1999 *Vortices in Nonlinear Fields* (Oxford: Oxford Science Publications)
[29] Pitaevskii L and Stringari S 2003 *Bose–Einstein Condensation* (Oxford: Oxford University Press)
[30] Pu H, Law C K, Eberly J H and Bigelow N 1999 Coherent disintegration and stability of vortices in trapped Bose condensates *Phys. Rev.* A **59** 1533–7
[31] Seman J A *et al* 2010 Three-vortex configurations in trapped Bose–Einstein condensates *Phys. Rev.* A **82** 033616
[32] Stringari S 1996 Collective excitations of a trapped Bose-condensed gas *Phys. Rev. Lett.* **77** 2360–3